LANGMUIR Article
Cite This: Langmuir 2018, 34, 4732−4738
pubs.acs.org/Langmuir

Mechanoresponsive Tuning of Anisotropic Wetting on Hierarchically Structured Patterns

Dokyeong Kwon,[†,‡] Sanghyuk Wooh,[§] Hyunsik Yoon,*[,∥] and Kookheon Char*[,†,‡]

[†]The National Creative Research Initiative Center for Intelligent Hybrids and [‡]The World Class University Program of Chemical Convergence for Energy and Environment, School of Chemical and Biological Engineering, College of Engineering, Seoul National University, Seoul 08826, Republic of Korea

[§]School of Chemical Engineering & Materials Science, Chung-Ang University, Seoul 06974, Republic of Korea

[∥]Department of Chemical and Biomolecular Engineering, Seoul National University of Science & Technology, Seoul 01811, Republic of Korea

Supporting Information

ABSTRACT: Here, we propose a simple mechanoresponsive system on patterned soft surfaces to manipulate both anisotropy and orientation of liquid wetting. On the poly(dimethylsiloxane) embedding line patterned structures, additional topographies, such as wrinkles and cracks, can be provided by applying compressive and tensile stress, respectively. This tunable hierarchy of structures with the different scales and directions of lines, wrinkles, and cracks allow the mechanoresponsive control of anisotropic wetting in a single platform. In addition, the wetting behavior on those surfaces is precisely investigated based on the concept of critical contact angle to overcome the ridges in a step flow.

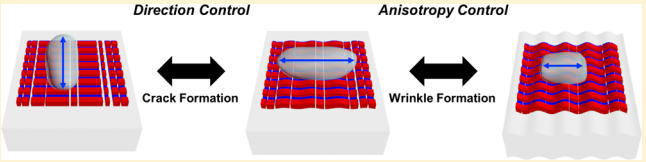

INTRODUCTION

Wetting studies on structured surfaces have gained intense interest because of their potential applications, such as water-repelling,[1−6] self-cleaning surfaces,[7−10] and water harvesting.[11−14] Various reports inspired by plants, insects, and even spider webs share the concept that the structure itself is the key to manipulating the wetting behavior by changing apparent interfacial correlations. Among these wetting characteristics, the anisotropic wetting found on rice leaves has been widely investigated for water guidance on the surface structures.[15−19] Rice leaves have hierarchically structured surfaces with microscale lines and nanoscale roughness. When water is placed on the surface, the water flows along the line patterns because there is an energy barrier to overcome in the perpendicular direction. This unique wetting property makes anisotropic surface patterns more interesting and indicates their potential to be extended into many practical applications such as painting, ink-jet printing, water harvesting, and microfluidics. Moreover, anisotropic studies have been extended to tunable wetting by mechanical[20−25] or electrical signals.[26] Chung et al.[20] used the wrinkling induced by releasing mechanical forces on the ultraviolet/ozone (UVO)-treated surface of prestrained poly(dimethylsiloxane) (PDMS) to give a direction to the flow along a one-dimensional pattern. When the UVO-treated PDMS was stretched again, the anisotropy disappeared as the wrinkled pattern disappeared. Other tunable anisotropic wetting studies have been reported using prepared hierarchical structures or dielectric elastomers for electrically responsive behaviors.[26] Most recently, there were a few reports on switching the axis of anisotropic wetting by mechanical stimuli. Rhee et al.[27] demonstrated a change in the wetting behavior by switching the orientation of the line patterns formed by soft skins with mechanical stretching. Additionally, Cha et al.[28] obtained fluidic networks by switching the direction of the capillary-driven water movement. Nevertheless, previous studies could only either control the degree of anisotropy or switch the direction of anisotropy in one system because of their plain structures. Here, we propose a method using hierarchical structures to manipulate the anisotropy itself as well as the orientation of the anisotropic wetting in one system. We prepared a line array with PDMS and realized microscale wrinkles or cracks by applying compressive or tensile stresses in the direction perpendicular to the line patterns. By controlling the competition between the energy barriers in the two orientations, we could change the shape of anisotropy during water movement. When we applied compressive strain to form wrinkles, we could control the anisotropy by balancing the barriers along the two axes. Because cracks had sharp edges compared with the line pattern, the direction of the smaller energy barrier was switched when the tensile strain was applied. We explained the energy barrier by the critical contact angle concept[29,30] and the experimental results showed a reasonable agreement. Furthermore, we prepared a prestrained and cracked hierarchical structure and demonstrated sequential control of the anisotropy by compressive strain and of the

Received: February 12, 2018
Revised: March 28, 2018
Published: March 29, 2018

DOI: 10.1021/acs.langmuir.8b00496
Langmuir 2018, 34, 4732−4738

orientation by tensile stress on a single hierarchically structured surface.

METHODS

Fabrication of Patterned PDMS. A silicon master with line/space patterns was prepared by conventional photolithography and dry etching process. The line width is 2400 nm, the spacing between lines is 800 nm, and the pattern height is 500 nm. The prepared silicon master was used as a basic mold to obtain multiple polyfluoropolyehter (PFPE) replica patterns. A PFPE replica mold was prepared by coating a mixture of PFPE prepolymers (5101X, Fluorolink) and an initiator onto the silicon master. We placed a transparent poly(ethylene terephthalate) film on the PFPE and exposed ultraviolet (UV) light (~55 s) to cure the PFPE. The cross-linked PFPE replica was carefully detached from the silicon master to generate the line/space patterns with 800 nm line patterns and 2400 nm spaces between the lines. Further UV treatment was applied for 3 h to fully cure the PFPE mold to ensure mechanical durability. A PDMS (Sylgard 184, Dow Corning) prepolymer 15:1-mixture (base: curing agent) was poured on the PFPE replica mold. After degassing and curing at 60 °C for 6 h, the PDMS sheets were detached from the replica mold. The resulting PDMS patterns have the identical line/space patterns with the silicon master because we performed the replica molding process twice.

Fabrication of Hierarchical Structures Based on Winkles. The patterned PDMS was placed in a handmade PDMS pull/press machine with which applied strain can be precisely controlled. After applying 1-D prestrain ranging from 0 to 40%, the patterned PDMS was UVO treated by a commercial UVO cleaner (Jelight Company Inc.) for 1 h. Because compressive stresses were applied to the PDMS sheets by releasing the prestrains, hierarchical structures of controlled microscale wrinkles embedding line patterns were obtained.

Fabrication of Hierarchical Structures Based on Cracks. The patterned PDMS was placed on the PDMS pull/press machine, without applying any prestrain. After UVO treatment for 1 h, 70−90% 1-D tensile strain was abruptly applied to form 1-D cracks. After the releasing step, a controlled tensile strain of 0−40% was then reapplied to control the hierarchical structures based on cracks.

Fabrication of Hierarchical Structures Based on Wrinkles and Cracks. The patterned PDMS was placed on the PDMS pull/press machine with 40% prestrain applied. After UVO treatment for 1 h, 70−90% 1-D tensile strain was abruptly applied to form 1-D cracks. Applying controlled tensile strain of 0−40% to the PDMS leads to combined hierarchical structures with both wrinkles and cracks. More detailed schematics of the fabrication of hierarchical structures are shown in Figure S1.

Characterizations. Surface structures were analyzed by observing the height profile obtained from ac-mode atomic force microscopy (AFM) images (NanoWizard 3, JPK Instruments). ac mode cantilevers (length = 125 μm, width = 30 μm) with an aluminum back coating were used. (ACTA, AppNano NanoStructures Inc.). All AFM images were taken in the size of 100 μm × 100 μm and with a scan rate of 0.4 Hz. Top-view photographs of anisotropic water droplets on hierarchical structures were obtained with a camera set over the PDMS pull/press machine and a syringe pump (KDS 100, KD Scientific) for flow control. Images for measuring drop anisotropy were taken with a fixed drop volume of 30 μL. (Anisotropy with other drop volumes is shown in Figure S2). Critical contact angles in the directions parallel and perpendicular to the line patterns were obtained through time-resolved contact angle analysis by taking images of advancing contact angles with a drop shape analysis system (DSA 100, Krüss GmbH). The maximum droplet volume was fixed to 10 μL, and the infuse rate was maintained at 10 μL min^{-1} for all video measurements.

RESULTS AND DISCUSSION

Figure 1 shows a schematic illustration of the concept of manipulating the isotropy and orientation of liquid droplets on surfaces with microscale wrinkles and cracks formed in the

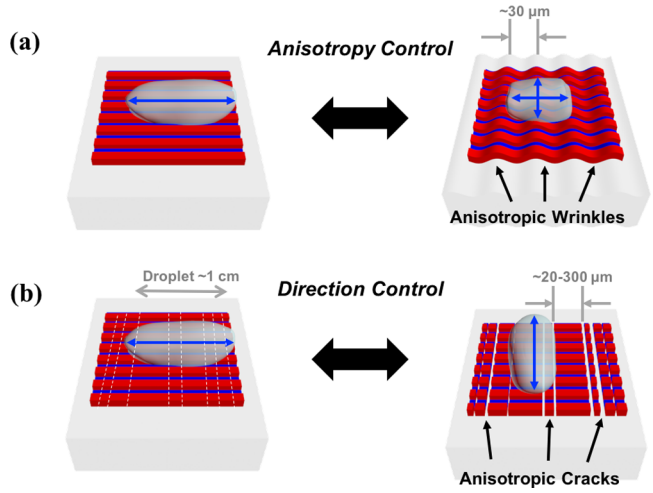

Figure 1. Conceptual illustrations of anisotropic wetting on the hierarchical structures originating from line patterns, wrinkles, and cracks. (a) Anisotropy of water can be controlled by wrinkling in the direction perpendicular to the line patterns. (b) Cracks on the line patterns can change the orientation of the anisotropic water droplet.

direction perpendicular to the line patterns. With the double replica molding method, we obtained a PDMS block with line patterns (2400 nm in line width, 800 nm in space). To realize wrinkles in the direction perpendicular to the line patterns (Figure 1a), we stretched this PDMS block in the direction parallel to the line patterns and then it exposed to UVO over the line patterns to form a stiff SiO_2 layer on top of the PDMS pattern. Next, we released the prestrain to apply compressive stress to the film. To obtain dual scale structures of cracks and line patterns, patterned PDMS was initially treated with UVO, without any prestrain being applied. Then, 70−90% tensile strain was abruptly applied to form cracks perpendicular to the direction of line patterns. It is well-known that cracks emerge when the applied tensile strain exceeds a critical value because of the mechanical fracture, which are anisotropic cracks vertical to the applied uniaxial tensile or bending strain.[31] When we release the strain and return to the original state, the cracks are closed. The white lines in Figure 1b represent the location of cracks after closing by the stress release. We harnessed the formation of micropatterns such as wrinkles or cracks, and their direction is perpendicular to the line pattern, which is the essential difference compared with other previous works.[27] As shown in Figure 1a, the water droplet lies asymmetrically along the line patterns when there are no mechanical forces. After applying compressive stress to form wrinkles in the perpendicular direction, the shape of the water droplet is changed to isotropic. When we generate cracks, as shown in Figure 1b, the anisotropic water droplet notably lies along the cracks, which indicates a change in the orientation of the asymmetric behavior.

Anisotropic Wetting Control Based on Wrinkle or Crack Formation. Figure 2a shows AFM images and the corresponding height profiles of the UVO-treated PDMS line patterns. When the compressive stress was applied by releasing the prestrain, microscale wrinkles were formed as shown in the AFM image in Figure 2b. The microscale wrinkles have a wavelength of ~30 μm, regardless of the applied prestrain, and the amplitude changes from 0 to 5.6 μm when the applied prestrain changes from 0 to 40%. From the characteristic

DOI: 10.1021/acs.langmuir.8b00496
Langmuir 2018, 34, 4732−4738

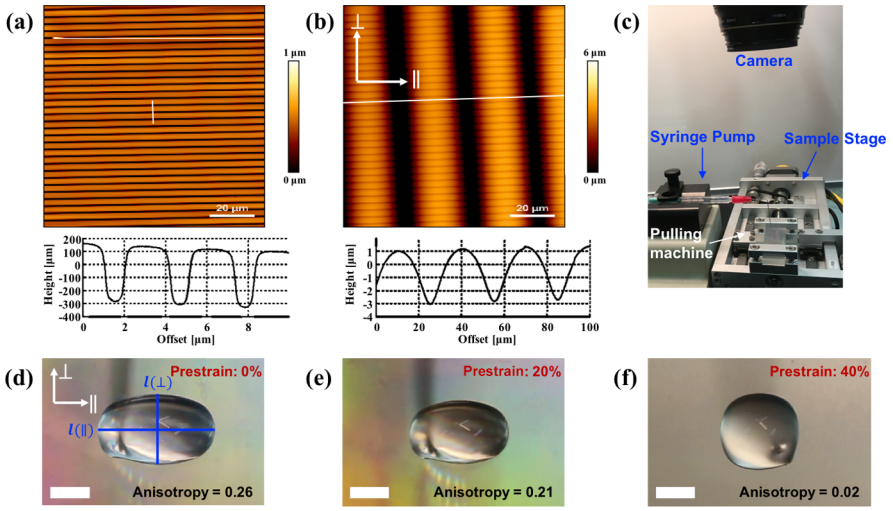

Figure 2. AFM images and height profile of line/space patterns (a) before and (b) after wrinkling. (c) Photograph of the liquid flow experimental apparatus, which can apply tensile strain to the prestrained samples. (d–f) Droplets exhibiting anisotropies of (d) 0.26, (e) 0.21, and (f) 0.02 on the line/space patterned surfaces with wrinkles on the perpendicular direction to the lines generated by different prestrain. The direction perpendicular to the line patterns is defined as ⊥, whereas the direction parallel to the line patterns is defined as ‖. Droplet anisotropy is defined as $[l(\|) - l(\perp)]/[l(\|) + l(\perp)]$, where $l(\|)$ and $l(\perp)$ represent the droplet length along the ‖ and ⊥ directions respectively. Each scale bar represents 2 mm.

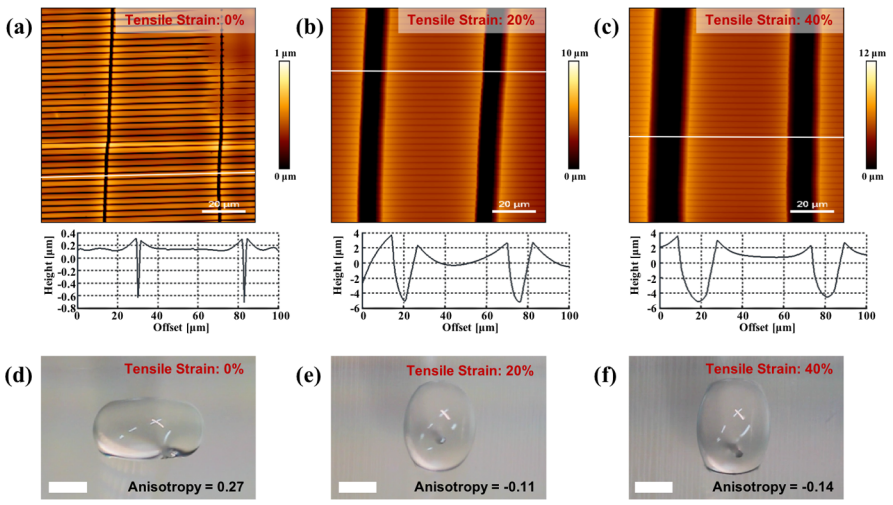

Figure 3. AFM images and the corresponding height profiles of line/space patterns (a) before applying tensile strain and (b) after applying 20% and (c) 40% tensile strain. (d) Top-view photograph of an anisotropic water droplet along the line patterns when there is no tensile strain. (e,f) Top-view photographs showing that the direction of the water droplets has changed from the original direction after applying 20 and 40% tensile strain, respectively. Each scale bar represents 2 mm.

wavelength of the wrinkles,[32−36] we could predict the thickness of the SiO_2 layer formed by UVO treatment by the relation

$$\text{Wavelength } \lambda = 2\pi h(E_f/3E_s)^{1/3} \quad (1)$$

where h is the thickness of the stiff layer, E_f is the modulus of the top film, and E_s is the modulus of the bottom elastomeric substrate. We assume that the UVO-treated top surface of PDMS is nearly isotropically changed to a stiff silicate top surface and that the bottom layer remains 15:1 PDMS ($E_s \approx 0.9$ MPa).[37−40] The calculated silicate layer thickness remains ∼0.3 μm, which agrees well with previous studies on the UVO treatment of PDMS surfaces.[37−40] Figure 2c shows an image of the experimental setup including the syringe pump (water infusion rate of 10 μL/min) and camera for observing the asymmetric behavior of a water droplet. A PDMS press/pull machine is placed under the syringe pump. Top-view optical images of water droplets were taken by the camera placed over vertical to the sample stage.

In most previous works reporting anisotropic wetting on various patterned surfaces,[15−18,23] researchers use the drop distortion parameter, which is defined as the ratio of the lengths of the major axis and minor axis. However, this parameter is valid only for systems in which the change in the major axis is inexistent, that is, there is no change in the wetting orientation, and information about wetting directions is excluded. In our system, it is necessary to redefine the droplet anisotropy using the normalized length ratio to include the anisotropy itself and the information about wetting orientation as follows

$$\text{Anisotropy} = \left[\frac{l(\|) - l(\perp)}{l(\|) + l(\perp)}\right] \quad (2)$$

DOI: 10.1021/acs.langmuir.8b00496
Langmuir 2018, 34, 4732−4738

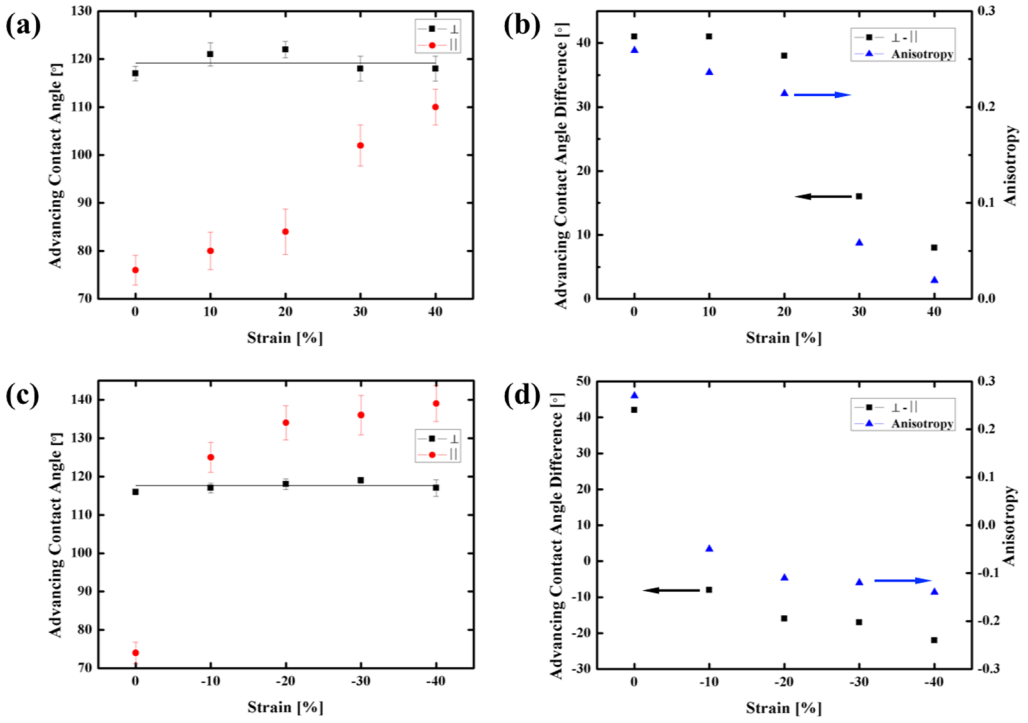

Figure 4. (a) Advancing contact angles in the direction parallel to the line patterns ($CA_{\parallel}$) increases as the compressive strain to form wrinkles increases, whereas the advancing angles in the direction perpendicular to the line patterns ($CA_{\perp}$) remains almost the same. (b) Difference of advancing contact angles in each direction of wrinkled surface shows similar trends as the droplet anisotropy. (c) Advancing contact angles in the direction parallel to the line patterns ($CA_{\parallel}$) increases as the tensile strain to form cracks increases, whereas the advancing angles in the direction perpendicular to the line patterns ($CA_{\perp}$) remains almost the same. (d) Difference of advancing contact angles in each direction of cracked surface shows similar trends as the droplet anisotropy.

When this parameter is positive, that is, the droplet length along the nanoscale line pattern direction is larger, the water droplet lies along the line patterns, whereas it has a negative sign when the water droplet lies along the direction of the microscale wrinkles or cracks.

Without any mechanical distortions of the UVO-treated patterned PDMS in Figure 2d, the water droplet wets along the line patterns, which describes the anisotropic wetting induced by the surface structures. In Figure 2e, the shape of the water droplet becomes more isotropic with the anisotropy of 0.21 than the droplet in Figure 2d with the anisotropy of 0.28. In addition, Figure 2f shows the droplet with an anisotropy of 0.02 even smaller than those of other two previous cases. This modified wetting behavior of water droplet is caused by the formation of wrinkles in the direction perpendicular to the line patterns. The wavelengths of wrinkles are about 8−10 times to the pitch of the line patterns, and the larger amplitude of wrinkles is formed by increasing the applied prestrain, affecting the anisotropy of wetting.

Besides wrinkle- and line-based hierarchical structures, by applying strain after the oxidation of line patterns, the hierarchical structures based on uniaxial cracks and line patterns can be fabricated (Figure 3a−c). By applying abrupt tensile strain of 70−90% to the oxidized line patterns, uniaxial cracks perpendicular to the line patterns emerge. When we further apply the tensile strain parallel to the line patterns after releasing the abrupt tensile strain, the width and the depth of the cracks can be controlled. Optical images of the anisotropic water droplets are shown in Figure 3d−f. When the tensile strain is small, the width of the crack remains small and the cracks are almost closed (Figure 3a). In this case, the anisotropy of the droplet remains positive, indicating that the direction of wetting remains parallel to the line patterns (Figure 3a). However, the cracks with wider widths by the increased tensile strain of over 20% influence the wetting property of the droplet (Figure 3b,c). On those surfaces, the droplet anisotropy changes to the negative value, which means that the direction of anisotropic wetting is changed to the direction along the cracks (Figure 3e,f) (more detailed droplet anisotropy measurements with varying droplet volumes are shown in Figure S2b, and the crack-to-crack distance distributions are shown in Figure S5).

The anisotropic shape of water droplets can be quantified by comparing the advancing contact angles both parallel and perpendicular to the line direction. Note that we measured the advancing contact angles because we examine the droplet shape while increasing the volume of the water droplet. This could be measured by taking snapshots during the dynamic contact angle measurement (Figure S3). Figure 4a shows that the wrinkled surfaces fabricated by the stronger applied prestrain exhibit the higher advancing contact angles of water parallel to the line patterns ($CA_{\parallel}$), whereas the advancing angles perpendicular to the line patterns ($CA_{\perp}$) show no significant changes. This result quantitatively agrees with previous works on anisotropic wetting studies based on wrinkles without any nanoscale features on the surface.[20,22,23] Figure 4b shows that the difference between the critical contact angles in each direction displays a similar tendency to the droplet anisotropy measured from the top-view optical images, which enables us to conclude that the advancing contact angle difference corresponds to the anisotropy of the water droplet. In case of the hierarchical structures based on microscale cracks and smaller line patterns, $CA_{\parallel}$ shows much bigger variation with varying applied tensile

DOI: 10.1021/acs.langmuir.8b00496
Langmuir 2018, 34, 4732−4738

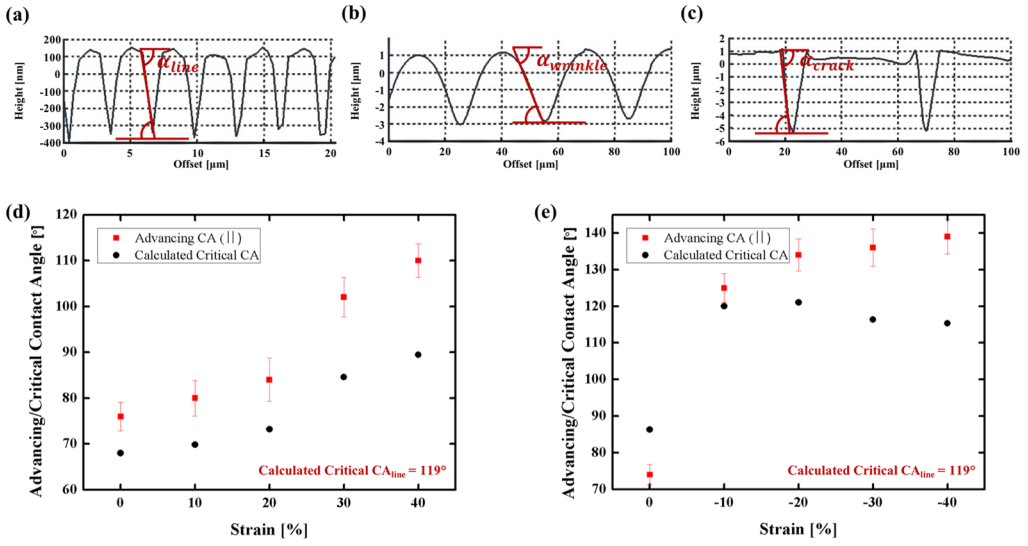

Figure 5. Characteristic height profiles from AFM for each (a) line pattern, (b) wrinkle, and (c) crack and the corresponding simplified groove angle (α) for each. (d,e) In both the wrinkle- and crack-based cases, the critical angles calculated from the height profiles show a similar tendency to the advancing contact angles.

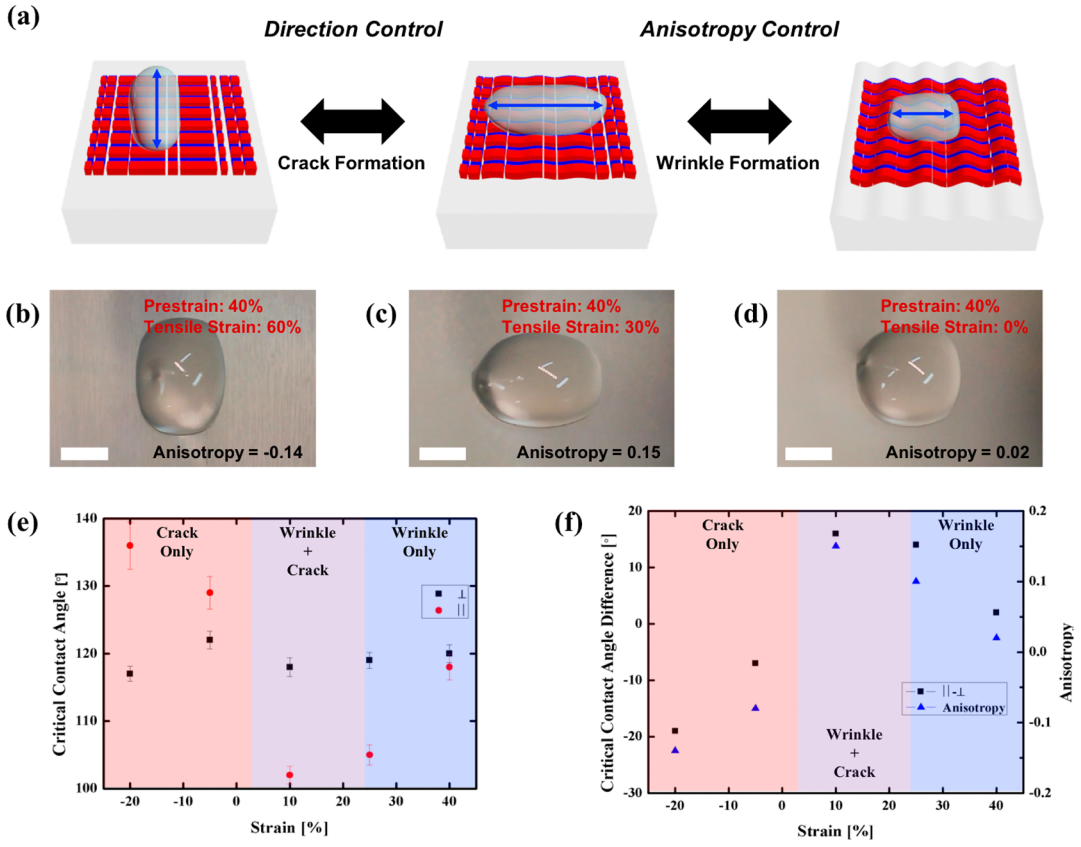

Figure 6. (a) Schematic illustration showing the mechanoresponsive tuning of the direction of an anisotropic water droplet with crack formation and the anisotropy of the droplet with wrinkle formation. (b) Top-view photograph of an anisotropic water droplet when the tensile strain is greater than prestrain, which leads to relatively large crack structures. (c) Top-view photograph of a water droplet when the tensile strain is similar to the prestrain, where the crack structures become negligible. (d) Top-view photograph of an anisotropic water droplet when the prestrain is greater than the tensile strain, which is the condition that induces wrinkle formation. Each scale bar represents 2 mm. (e) Effect of the strain on the advancing contact angles and the droplet anisotropy on hierarchical structures based on both wrinkles and cracks. When the applied strain is small, which leads to large crack features, the advancing contact angles perpendicular to the strain are larger. As the strain increases, the closing of the cracks changes the direction of wetting, and the anisotropy of the water droplet can be controlled in the same way as when only wrinkles are present. (f) Differences in the advancing contact angle in each direction and the flow anisotropy show similar trends as the strain is varied.

DOI: 10.1021/acs.langmuir.8b00496
Langmuir 2018, 34, 4732−4738

strain than in the case of the hierarchical structures based on wrinkles and line patterns which are controlled with varying compressive prestrain, whereas $CA_{\perp}$ remain almost constant (Figure 4c). When we apply tensile strain (greater than ~10%), $CA_{\parallel}$ shows larger values than $CA_{\perp}$, which is in good agreement with the orientation change in droplet anisotropy, as shown in Figure 4d.

To explain the anisotropic wetting phenomena on groove-like patterns, Oliver et al. introduced the critical contact angle concept.[29] The critical contact angle is defined as the contact angle at the moment when a water droplet moves over to the next periodic pattern after pinning on the former pattern, which is identical to the advancing contact angle on grooved surfaces. We could calculate the critical contact angles from the surface height profiles of the line patterns, (Figure 5a) wrinkle patterns (Figure 5b), and crack patterns (Figure 5c). The microscopic definition of critical contact angles given by Oliver et al. is

$$\text{Critical contact angle (CA) } \theta_{cr} = \theta + \alpha \tag{3}$$

where θ is the static contact angle on the flat surface, and α is the inclination of the simplified pattern. (Figure S4a) For 1 h UVO-treated PDMS examined in this study, $\theta = 68°$ (Figure S4b). We defined the simplified pattern inclination α for each system as following, (Figure 5a–c)

$$\alpha_{line} = \tan^{-1}\frac{(\text{depth})}{(\text{pitch}/2)} \tag{4}$$

$$\alpha_{wrinkle} = \tan^{-1}\frac{(\text{amplitude})}{(\text{wavelength}/2)} \tag{5}$$

$$\alpha_{crack} = \tan^{-1}\frac{(\text{depth})}{(\text{width}/2)} \tag{6}$$

The calculated critical contact angle for the line pattern, 119°, agrees well with the advancing contact angle of $CA_{\perp}$, which confirms that the critical angle concept gives us proper insights into the anisotropic wetting phenomena. We further confirm that the calculated critical contact angles of the wrinkle patterns and crack patterns show a similar trend with the advancing contact angles of $CA_{\parallel}$ for each system (Figure 5d,e).

Orientation and Anisotropy Control by Combination of Wrinkles and Cracks on Line Patterns. By combining the concepts of tunable hierarchies based on the formation of wrinkles and cracks in the presence of line patterns, we demonstrate a method to control both orientation and anisotropy of a water droplet in a single system. We prepared the patterned PDMS that is UVO-treated after applying prestrain (AFM images and representative height profiles are shown in Figure S6). Then, we generated cracks by abruptly applying a tensile strain of 70–90% which is much greater than the prestrain. After the procedure, we examine the anisotropic behavior of the water droplet by increasing the volume of the droplet. When the tensile strain is greater than the prestrain, the water droplet shows an anisotropic form along the generated cracks as shown in Figure 6a,b. When the applied tensile strain and the prestrain are similar, the direction of the water droplet follows the lines because there are no significant wrinkles or cracks (Figure 6a,c). By contrast, when there is no tensile strain applied, wrinkles become dominant, and the shape of the water droplet is isotropic (Figure 6a,d).

Figure 6e shows the advancing contact angles in directions both perpendicular and parallel to the line patterns of this system. As we discussed previously regarding systems with only wrinkles or cracks, the advancing contact angles perpendicular to the line patterns ($CA_{\perp}$) show little variation. Conversely, the critical contact angles parallel to the line patterns ($CA_{\parallel}$) vary with applied strain and can be classified into three regimes (Figure 6e,f). When the tensile strain is greater than the prestrain, only cracks are formed, and the critical contact angle across the cracks becomes higher than that along the line patterns. This indicates that the energy barrier across the line patterns is smaller than that across the cracks. If the applied tensile strain becomes similar to the prestrain, the advancing contact angle along the line patterns is the highest, which means that the energy barrier of the line patterns is dominant and that the direction of anisotropic wetting can be controlled. Furthermore, when the applied prestrain is dominant, the wetting phenomenon is governed by the wrinkles as well as by the line patterns, and the shape of the water droplet becomes isotropic, thus enabling the system to control anisotropy also.

CONCLUSIONS

In this work, mechanoresponsive anisotropic wetting was demonstrated that can control both anisotropy and orientation by using tunable hierarchical structures based on wrinkles (wavelength: ~30 μm, amplitude: 0–5.6 μm) and cracks (width: 1–16 μm) in the presence of a line pattern (width: ~2.4 μm). Compressive or tensile stress was applied to the UVO-treated PDMS with line patterns to generate wrinkles or cracks in the direction perpendicular to the line patterns. We could simply manipulate the anisotropy of the water droplets on the line patterned surface by tuning the amplitudes of wrinkles and the orientation of the droplets by tuning the widths of cracks. In addition, we measured advancing contact angles to explain the anisotropy change with a concept of a critical contact angle. Moreover, the combined effects of the wrinkles and cracks on the anisotropic wetting enabled control of both anisotropy and orientation of water droplets in a single platform. We believe that this concept of mechanoresponsive anisotropic wetting can be easily applicable to various anisotropic wetting applications such as microfluidics and water harvestings and propose a new way to develop tunable anisotropic wetting surfaces.

ASSOCIATED CONTENT

Supporting Information

The Supporting Information is available free of charge on the ACS Publications website at DOI: 10.1021/acs.langmuir.8b00496.

Figures S1–S6 (PDF)

AUTHOR INFORMATION

Corresponding Authors

*E-mail: hsyoon@seoultech.ac.kr (H.Y.).
*E-mail: khchar@snu.ac.kr (K.C.).

ORCID

Sanghyuk Wooh: 0000-0002-6535-370X
Hyunsik Yoon: 0000-0002-6602-369X
Kookheon Char: 0000-0002-7938-8022

Notes

The authors declare no competing financial interest.

DOI: 10.1021/acs.langmuir.8b00496
Langmuir 2018, 34, 4732–4738

■ ACKNOWLEDGMENTS

This work has been supported by the National Creative Research Initiative Program for "Intelligent Hybrids Research Center" (no. 2010-0018290) funded by the Korea Ministry of Science, ICT & Future Planning (MSIP), by a National Research Foundation of Korea (NRF) grant, the BK21 Plus Program in SNU Chemical Engineering and the Commercialization Promotion Agency for R&D Outcomes Grant funded by the Korean Government (MSIP) (2015, Joint Research Corporations Support Program).

■ REFERENCES

(1) Nakajima, A.; Hashimoto, K.; Watanabe, T. Recent Studies on Super-Hydrophobic Films. *Monatsh. Chem.* **2001**, *132*, 31−41.
(2) Quéré, D. Surface chemistry: Fakir droplets. *Nat. Mater.* **2002**, *1*, 14−15.
(3) Erbil, H. Y.; Demirel, A. L.; Avcı, Y.; Mert, O. Transformation of a Simple Plastic into a Superhydrophobic Surface. *Science* **2003**, *299*, 1377−1380.
(4) Kim, Y. H.; Lee, Y. M.; Lee, J. Y.; Ko, M. J.; Yoo, P. J. Hierarchical Nanoflake Surface Driven by Spontaneous Wrinkling of Polyelectrolyte/Metal Complexed Films. *ACS Nano* **2012**, *6*, 1082−1093.
(5) Ma, W.; Wu, H.; Higaki, Y.; Otsuka, H.; Takahara, A. A "Non-Sticky" Superhydrophobic Surface Prepared by Self-Assembly of Fluoroalkyl Phosphonic Acid on a Hierarchically Micro/Nanostructured Alumina Gel Film. *Chem. Commun.* **2012**, *48*, 6824−6826.
(6) Xu, L.; He, J. Fabrication of Highly Transparent Superhydrophobic Coatings from Hollow Silica Nanoparticles. *Langmuir* **2012**, *28*, 7512−7518.
(7) Blossey, R. Self-Cleaning Surfaces - Virtual Realities. *Nat. Mater.* **2003**, *2*, 301−306.
(8) Hong, J.; Bae, W. K.; Lee, H.; Oh, S.; Char, K.; Caruso, F.; Cho, J. Tunable Superhydrophobic and Optical Properties of Colloidal Films Coated with Block-Copolymer-Micelles/Micelle-Multilayers. *Adv. Mater.* **2007**, *19*, 4364−4369.
(9) Karunakaran, R. G.; Lu, C.-H.; Zhang, Z.; Yang, S. Highly Transparent Superhydrophobic Surfaces from the Coassembly of Nanoparticles (≤100 nm). *Langmuir* **2011**, *27*, 4594−4602.
(10) Wooh, S.; Koh, J. H.; Lee, S.; Yoon, H.; Char, K. Trilevel-Structured Superhydrophobic Pillar Arrays with Tunable Optical Functions. *Adv. Funct. Mater.* **2014**, *24*, 5550−5556.
(11) Lopez, G.; Biebuyck, H.; Frisbie, C.; Whitesides, G. Imaging of Features on Surfaces by Condensation Figures. *Science* **1993**, *260*, 647.
(12) Parker, A. R.; Lawrence, C. R. Water Capture by a Desert Beetle. *Nature* **2001**, *414*, 33−34.
(13) Zhai, L.; Berg, M. C.; Cebeci, F. Ç.; Kim, Y.; Milwid, J. M.; Rubner, M. F.; Cohen, R. E. Patterned Superhydrophobic Surfaces: Toward a Synthetic Mimic of the Namib Desert Beetle. *Nano Lett.* **2006**, *6*, 1213−1217.
(14) Kim, G.-T.; Gim, S.-J.; Cho, S.-M.; Koratkar, N.; Oh, I.-K. Wetting-Transparent Graphene Films for Hydrophobic Water-Harvesting Surfaces. *Adv. Mater.* **2014**, *26*, 5166−5172.
(15) Zhao, Y.; Lu, Q.; Li, M.; Li, X. Anisotropic Wetting Characteristics on Submicrometer-Scale Periodic Grooved Surface. *Langmuir* **2007**, *23*, 6212−6217.
(16) Xia, D.; Brueck, S. R. J. Strongly Anisotropic Wetting on One-Dimensional Nanopatterned Surfaces. *Nano Lett.* **2008**, *8*, 2819−2824.
(17) Chu, K.-H.; Xiao, R.; Wang, E. N. Uni-Directional Liquid Spreading on Asymmetric Nanostructured Surfaces. *Nat. Mater.* **2010**, *9*, 413−417.
(18) Neuhaus, S.; Spencer, N. D.; Padeste, C. Anisotropic Wetting of Microstructured Surfaces as a Function of Surface Chemistry. *ACS Appl. Mater. Interfaces* **2012**, *4*, 123−130.
(19) Hancock, M. J.; Demirel, M. C. Anisotropic Wetting on Structured Surfaces. *MRS Bull.* **2013**, *38*, 391−396.
(20) Chung, J. Y.; Youngblood, J. P.; Stafford, C. M. Anisotropic Wetting on Tunable Micro-Wrinkled Surfaces. *Soft Matter* **2007**, *3*, 1163−1169.
(21) Lin, P.-C.; Yang, S. Mechanically Switchable Wetting on Wrinkled Elastomers with Dual-Scale Roughness. *Soft Matter* **2009**, *5*, 1011−1018.
(22) Lee, S. G.; Lim, H. S.; Lee, D. Y.; Kwak, D.; Cho, K. Tunable Anisotropic Wettability of Rice Leaf-Like Wavy Surfaces. *Adv. Funct. Mater.* **2013**, *23*, 547−553.
(23) Goel, P.; Kumar, S.; Sarkar, J.; Singh, J. P. Mechanical Strain Induced Tunable Anisotropic Wetting on Buckled PDMS Silver Nanorods Arrays. *ACS Appl. Mater. Interfaces* **2015**, *7*, 8419−8426.
(24) Roy, P. K.; Pant, R.; Nagarajan, A. K.; Khare, K. Mechanically Tunable Slippery Behavior on Soft Poly(dimethylsiloxane)-Based Anisotropic Wrinkles Infused with Lubricating Fluid. *Langmuir* **2016**, *32*, 5738−5743.
(25) Shao, Z.-C.; Zhao, Y.; Zhang, W.; Cao, Y.; Feng, X.-Q. Curvature Induced Hierarchical Wrinkling Patterns in Soft Bilayers. *Soft Matter* **2016**, *12*, 7977−7982.
(26) Jun, K.; Kim, D.; Ryu, S.; Oh, I.-K. Surface Modification of Anisotropic Dielectric Elastomer Actuators with Uni- and Bi-axially Wrinkled Carbon Electrodes for Wettability Control. *Sci. Rep.* **2017**, *7*, 6091.
(27) Rhee, D.; Lee, W.-K.; Odom, T. W. Crack-Free, Soft Wrinkles Enable Switchable Anisotropic Wetting. *Angew. Chem., Int. Ed.* **2017**, *56*, 6523−6527.
(28) Cha, J.; Shin, H.; Kim, P. Crack/Fold Hybrid Structure-Based Fluidic Networks Inspired by the Epidermis of Desert Lizards. *ACS Appl. Mater. Interfaces* **2016**, *8*, 28418−28423.
(29) Oliver, J. F.; Huh, C.; Mason, S. G. Resistance to Spreading of Liquids by Sharp Edges. *J. Colloid Interface Sci.* **1977**, *59*, 568−581.
(30) Kim, S. M.; Kang, D. H.; Koh, J. H.; Suh, H. S.; Yoon, H.; Suh, K.-Y.; Char, K. Thermoresponsive Switching of Liquid Flow Direction on a Two-Face Prism Array. *Soft Matter* **2013**, *9*, 4145−4149.
(31) Kim, H.-N.; Lee, S.-H.; Suh, K.-Y. Controlled Mechanical Fracture for Fabricating Microchannels with Various Size Gradients. *Lab Chip* **2011**, *11*, 717−722.
(32) Bowden, N.; Huck, W. T. S.; Paul, K. E.; Whitesides, G. M. The Controlled Formation of Ordered, Sinusoidal Structures by Plasma Oxidation of an Elastomeric Polymer. *Appl. Phys. Lett.* **1999**, *75*, 2557−2559.
(33) Groenewold, J. Wrinkling of Plates Coupled with Soft Elastic Media. *Phys. A* **2001**, *298*, 32−45.
(34) Stafford, C. M.; Harrison, C.; Beers, K. L.; Karim, A.; Amis, E. J.; VanLandingham, M. R.; Kim, H.-C.; Volksen, W.; Miller, R. D.; Simonyi, E. E. A Buckling-Based Metrology for Measuring the Elastic Moduli of Polymeric Thin Films. *Nat. Mater.* **2004**, *3*, 545−550.
(35) Huang, Z. Y.; Hong, W.; Suo, Z. Nonlinear Analyses of Wrinkles in a Film Bonded to a Compliant Substrate. *J. Mech. Phys. Solids* **2005**, *53*, 2101−2118.
(36) Khang, D.-Y.; Rogers, J. A.; Lee, H. H. Mechanical Buckling: Mechanics, Metrology, and Stretchable Electronics. *Adv. Funct. Mater.* **2009**, *19*, 1526−1536.
(37) Efimenko, K.; Wallace, W. E.; Genzer, J. Surface Modification of Sylgard-184 Poly(dimethyl siloxane) Networks by Ultraviolet and Ultraviolet/Ozone Treatment. *J. Colloid Interface Sci.* **2002**, *254*, 306−315.
(38) Özçam, A. E.; Efimenko, K.; Genzer, J. Effect of Ultraviolet/Ozone Treatment on the Surface and Bulk Properties of poly-(dimethyl siloxane) and poly(vinylmethyl siloxane) Networks. *Polymer* **2014**, *55*, 3107−3119.
(39) Glatz, B. A.; Tebbe, M.; Kaoui, B.; Aichele, R.; Kuttner, C.; Schedl, A. E.; Schmidt, H.-W.; Zimmermann, W.; Fery, A. Hierarchical Line-Defect Patterns in Wrinkled Surfaces. *Soft Matter* **2015**, *11*, 3332−3339.
(40) Wilder, E. A.; Guo, S.; Lin-Gibson, S.; Fasolka, M. J.; Stafford, C. M. Measuring the Modulus of Soft Polymer Networks via a Buckling-Based Metrology. *Macromolecules* **2006**, *39*, 4138−4143.

DOI: 10.1021/acs.langmuir.8b00496
Langmuir 2018, 34, 4732−4738